




Article

Control of Eu Oxidation State in $Y_2O_{3-x}S_x:Eu$ Thin-Film Phosphors Prepared by Atomic Layer Deposition: A Structural and Photoluminescence Study

José Rosa ¹, Jonas Deuermeier ² , Pekka J. Soininen ¹, Markus Bosund ¹, Zhen Zhu ¹, Elvira Fortunato ², Rodrigo Martins ², Mutsumi Sugiyama ³  and Saoussen Merdes ^{1,*} 

¹ Beneq Oy, Olarinluoma 9, FI-02200 Espoo, Finland; jose.rosa@beneq.com (J.R.);

pekka.j.soininen@beneq.com (P.J.S.); markus.bosund@beneq.com (M.B.); zhen.zhu@beneq.com (Z.Z.)

² i3N/CENIMAT, Department of Materials Science, Faculty of Sciences and Technology, Universidade NOVA de Lisboa and CEMOP/UNINOVA, Campus de Caparica, 2829-516 Caparica, Portugal; j.deuermeier@campus.fct.unl.pt (J.D.); emf@fct.unl.pt (E.F.); rfpm@fct.unl.pt (R.M.)

³ Department of Electrical Engineering, Tokyo University of Science, 2641 Yamazaki, Noda, Chiba 278-8510, Japan; mutsumi@rs.noda.tus.ac.jp

* Correspondence: saoussen.merdes@beneq.com

Received: 12 November 2019; Accepted: 19 December 2019; Published: 23 December 2019



Abstract: Structural and photoluminescence studies were carried out on Eu-doped $Y_2O_{3-x}S_x$ thin films grown by atomic layer deposition at 300 °C. $(CH_3Cp)_3Y$, H_2O , and H_2S were used as yttrium, oxygen, and sulfur precursors, respectively, while $Eu(thd)_3$ was used as the europium precursor. The Eu oxidation state was controlled during the growth process by following the $Eu(thd)_3$ pulse with either a H_2S or O_3 pulse. The $Eu(thd)_3/O_3$ pulse sequence led to photoluminescence emission above 550 nm, whereas the $Eu(thd)_3/H_2S$ pulse sequence resulted in emission below 500 nm.

Keywords: $Y_2O_2S:Eu$; Eu oxidation state; phosphor; photoluminescence

1. Introduction

The study of red- and blue-emitting phosphors has major importance in the luminescence field due to the need for a wider color gamut in current displays and an increase in the efficiency of optoelectronic devices. Most of the studies on luminescent materials are carried out using luminescent lanthanide ions [1,2]. This choice is supported by high-intensity sharp line emission, persistent phosphorescence, and good luminescence efficiency generated by the d–f and f–f transitions [3].

The emission of various colors can be generated by doping a semiconductor matrix with different lanthanide ions that act as luminescent centers [4]. The trivalent europium ion (Eu^{3+}) is the main choice to achieve red color emission. The strong emission is due to the intensive $^5D_0 \rightarrow ^7F_2$ electronic transition which generates a wavelength of 610–630 nm, depending on the host semiconductor matrix [5,6]. Europium can also assume a divalent state of oxidation (Eu^{2+}) and can act as an important luminescent center. It is known for its broad emission band between ultraviolet and red, where the dominant emission of Eu^{2+} ions is attributed to the $^4f_6^5d_1 \rightarrow ^4f_7$ transition [7]. Many papers have reported Eu^{2+} -doped material systems such as fluorides [8], chlorides [9], bromides [10], oxides [11], selenides [12], iodides [13], nitrides [14], and sulfides [15]. Because Eu^{2+} is highly dependent on the environment, each material emits in a specific range [7].

$Y_2O_2S:Eu$ is a well-known phosphor which has mainly been investigated as a host for Eu^{3+} in order to obtain red emission [5,16–21]. This is supported by the similar dimensions of Eu^{3+} and Y^{3+}

ionic radii of 1.01 Å and 0.96 Å at room temperature, respectively [22]. $Y_2O_2S:Eu^{3+}$ was first reported by Hardy as a substitution for yttrium orthovanadate due to its high emission efficiency [23]. Since then, it has been studied and used in luminescence applications such as light-emitting diodes [24] and field emission displays [4].

During the last decade, Y_2O_2S doped with europium was successfully grown by several techniques including pulsed laser deposition [16], hydrothermal method [5], sol-gel template method [19], and decomposition method [17]. However, when using these growth techniques, the europium dopant tends to oxidize to its trivalent form Eu^{3+} , as the divalent Eu^{2+} is unlikely to exist in Y_2O_2S , according to energy level considerations. This results in red being the main emission color generated by the $Y_2O_2S:Eu$ material.

In this work, it is shown that the oxidation state of Eu in the $Y_2O_{3-x}S_x$ (YOS) matrix can be controlled through the doping configuration by using the atomic layer deposition (ALD) method. Thus, during the growth process, Eu atoms on the surface were deliberately exposed to either oxidizing O_3 or reducing H_2S gas in order to generate a trivalent or a divalent oxidation state of Eu, respectively. This led to either red or violet/blue color emission from $Y_2O_{3-x}S_x:Eu$ (YOS:Eu).

2. Materials and Methods

$Y_2O_{3-x}S_x:Eu$ thin films were grown at 300 °C on (100)-oriented Si substrates using atomic layer deposition. The processes were carried out in a Beneq TFS-200 ALD-reactor (Beneq Oy, Espoo, Finland). $(CH_3Cp)_3Y$ (98%, Intatrade, Anhalt-Bitterfeld Germany), H_2O , and H_2S were used as yttrium, oxygen, and sulfur precursors, respectively, whereas $Eu(thd)_3$ (99.9%, Strem Chemicals, Kehl, Germany) was used as the Eu dopant precursor. N_2 was used as the carrier and purging gas. Eu was introduced into the $Y_2O_{3-x}S_x$ matrix in combination with either H_2S or O_3 . During the processes, the pressure in the reactor was about 2 mbar. Process steps and parameters, including pulse sequences and pulse time, are summarized in Figure 1 and Table 1. Note that an N_2 purge step was applied in all processes after each pulse. The purge time was 7 s.

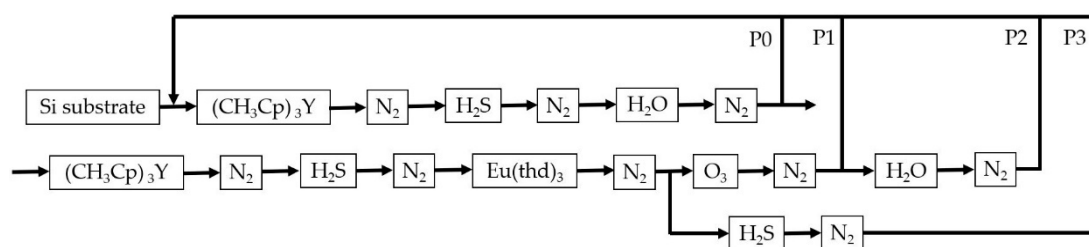


Figure 1. Schematic diagram of the processes used for the growth of the films.

Table 1. Pulse sequences and corresponding pulsing times for $Y_2O_{3-x}S_x/Y_2O_{3-x}S_x:Eu$ atomic layer deposition (ALD) processes.

Process	Pulse Sequence	Pulse Time (s)
P0	$(CH_3Cp)_3Y/H_2S/H_2O$	2.5/0.5/0.15
P1	$(CH_3Cp)_3Y/H_2S/H_2O/(CH_3Cp)_3Y/H_2S/Eu(thd)_3/O_3$	2.5/0.5/0.15/2.5/0.5/2.5/3
P2	$(CH_3Cp)_3Y/H_2S/H_2O/(CH_3Cp)_3Y/H_2S/Eu(thd)_3/O_3/H_2O$	2.5/0.5/0.15/2.5/0.5/2.5/3/0.15
P3	$(CH_3Cp)_3Y/H_2S/H_2O/(CH_3Cp)_3Y/H_2S/Eu(thd)_3/H_2S$	2.5/0.5/0.15/2.5/0.5/2.5/0.5

The thickness of the grown films was determined with a SENTECH SE400adv ellipsometer (SENTECH Instruments GmbH, Berlin, Germany), using a 633 nm wavelength at 70° angle of incidence. The crystallinity was investigated by X-ray diffraction (XRD) using Cu $K\alpha$ line in a Rigaku SmartLab (Rigaku Europe SE, Neu-Isenburg, Germany) high-resolution X-ray diffractometer. Chemical analyses were carried out by X-ray photoelectron spectroscopy (XPS). The spectra were measured with a Kratos Axis Supra spectrometer (Kratos Analytical Ltd., Manchester, UK), employing a monochromatic Al $K\alpha$ source running at 225 W. The detailed spectra were either recorded at 10 eV pass energy for improved

energy resolution or at 40 eV for faster acquisition (decreased X-ray exposure). Photoluminescence measurements were carried out at room temperature in a Perkin Elmer LS55 spectrophotometer (PerkinElmer Inc., Waltham, MA, USA), equipped with a pulsed Xenon discharge lamp of power equivalent to 20 kW for 8 μ s duration. The samples were excited using two wavelengths, 266 and 355 nm.

3. Results

Figure 1 shows the schematic diagram of the ALD processes used for the growth of the $Y_2O_{3-x}S_x$ and $Y_2O_{3-x}S_x:Eu$ thin films. Films with thicknesses between 50 and 300 nm were thus grown using the parameters summarized in Table 1. Thickness variations measured on about 50-nm-thick samples using ellipsometry were used to verify film homogeneity. Process P1, where the $Eu(thd)_3$ pulse was followed by the O_3 pulse, resulted in poor homogeneity with thickness fluctuations reaching 19%. The additional pulse of H_2O after the O_3 pulse in process P2 resulted in better thickness homogeneity with fluctuations down to about 10%. Due to the better film quality with process P2, in addition to processes P0 and P3, results related to films prepared with a combination of O_3/H_2O when introducing the Eu dopant in the matrix are presented. Therefore, in what follows, unless stated otherwise, the additional H_2O pulse step is assumed when the $Eu(thd)_3/O_3$ pulse sequence related results are discussed.

3.1. Crystallinity

Figure 2 shows XRD patterns measured between 20° and 60° at a fixed grazing incidence angle of 1° on samples grown using processes P0, P2, and P3. The undoped YOS sample and the Eu-doped one grown using the $Eu(thd)_3/O_3$ pulse sequence showed a single very broad peak around 30° , suggesting that the layers had a rather amorphous structure. However, the sample grown using the $Eu(thd)_3/H_2S$ pulse sequence showed several sharp peaks, indicating that the film had a crystalline structure. Using JCPDS file no. 24-1424, $Y_2O_{3-x}S_x$ -related (100), (101), (102), (003), (110), (103), (112), and (201) reflections were identified, indicating that YOS:Eu grown using the $Eu(thd)_3/H_2S$ pulse sequence had a hexagonal crystal structure with the lattice parameters $a = 3.794 \text{ \AA}$ and $c = 6.580 \text{ \AA}$.

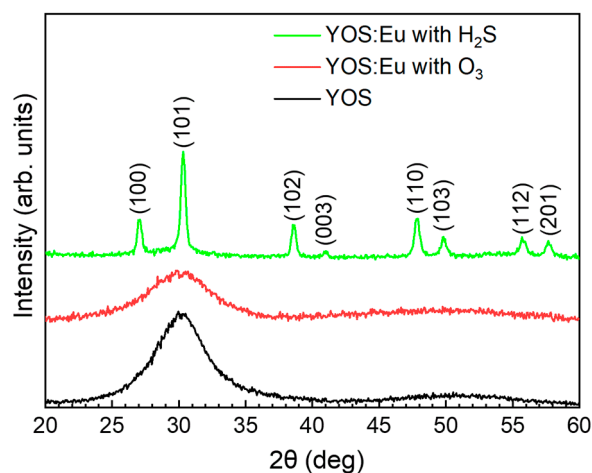


Figure 2. XRD of samples prepared using processes P0, P2, and P3.

3.2. Chemical Analyses

An XPS overview spectrum (figure not shown) showed carbon, yttrium, oxygen, and sulfur in all the samples, as well as europium in the doped ones. Sputter cleaning was not carried out in order to avoid the introduction of surface carbon contamination into the layers. Charge accumulation took place due to the high resistivity of the material, which led to a shift of the peaks. The position of C, Y, O, and S core levels was corrected. A change in the Eu oxidation state from Eu^{2+} to Eu^{3+} during the measurement was also observed. Due to the uncertainty of the Eu oxidation state during the XPS

measurements, spectra related to Eu core levels were not analyzed in detail. Nevertheless, Eu 3d core level spectra were used in the estimation of the elemental composition of the doped films.

Figure 3a shows measured and fitted XPS spectra for C 1s core levels in YOS and YOS:Eu films prepared by processes P0, P2, and P3. The spectra were deconvoluted by fitting the measured core level peaks with Voigt function. The corresponding binding energies are displayed in Figure 3a,b. C 1s core level spectra were composed of four peaks that were attributed mainly to CO_3^{2-} and carbon contamination. In addition to the CO_3^{2-} peak [25], all the samples showed C–C, C–O–C, and O–C=O bonds [25,26]. Figure 3b shows the S 2s core level spectra measured in the same samples. The spectra showed a significant difference between the sulfur bonds, depending on the growth process: while sulfate bonds ($\text{Y}_2(\text{SO}_4)_3$) [27] were dominant in the YOS and YOS:Eu prepared using the $\text{Eu}(\text{thd})_3/\text{O}_3$ sequence, sulfide bonds were identified only in the YOS:Eu film prepared using $\text{Eu}(\text{thd})_3/\text{H}_2\text{S}$ pulse sequence.

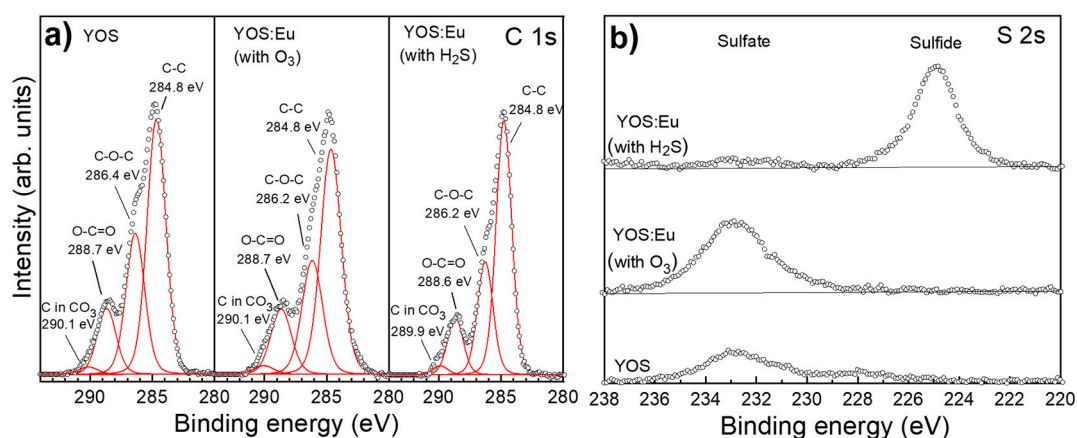


Figure 3. Measured and fitted (a) C 1s and (b) S 2s core level spectra. The films were prepared by processes P0, P2, and P3. Open symbols represent measured spectra, whereas red lines show fitting results.

In Table 2, the elemental compositions of YOS:Eu samples, where Eu was introduced into the matrix in combination with either O₃ (process P2) or H₂S (process P3), are compared. C 1s, Eu 3d, O 1s, S 2s, and Y 3p core level spectra were used for the calculations. The film grown using the $\text{Eu}(\text{thd})_3/\text{O}_3$ pulse sequence had a higher oxygen content than the one grown using the $\text{Eu}(\text{thd})_3/\text{H}_2\text{S}$ sequence, with an O/S ratio of 8.1 and 5.7, respectively. While the europium and yttrium contents were found to be lower in the sample prepared using O₃, the carbon content was nearly the same in both films. Note that the carbon concentration measured by XPS was relatively high, with values exceeding 30%.

Table 2. Comparison of the elemental composition of Eu-doped $\text{Y}_2\text{O}_{3-x}\text{S}_x$ films prepared using $\text{Eu}(\text{thd})_3/\text{O}_3$ and $\text{Eu}(\text{thd})_3/\text{H}_2\text{S}$ pulse sequences.

Process	Y (at.%)	O (at.%)	S (at.%)	C (at.%)	Eu (at.%)
P2	10.6	48.7	6.0	30.8	3.9
P3	14.7	39.7	6.9	31.0	7.7

Figure 4a,b shows the measured and fitted XPS spectra for Y 3d core levels in YOS and YOS:Eu films prepared using the $\text{Eu}(\text{thd})_3/\text{O}_3$ pulse sequence, respectively. Figure 4c shows the spectra for Y 3d together with S 2p core levels in YOS:Eu films prepared using the $\text{Eu}(\text{thd})_3/\text{H}_2\text{S}$ sequence. The measured spectra were fitted using Voigt function. Based on the results extracted from Figure 2, the following fitting restraints were applied:

- For Y 3d (5/2 and 3/2) doublets, a constant ratio of 3:2 and a constant separation distance of 2.05 eV were applied, whereas for S 2p (3/2 and 1/2) doublets, a constant ratio of 2:1 and a constant separation distance of 1.18 eV were applied.
- For YOS:Eu sample prepared using the Eu(thd)₃/H₂S pulse sequence, the sulfide 2p and the Y₂(SO₄)₃ 3d peak area ratio were fixed to the values determined from the S 2s fit in Figure 2.
- Using the NIST (National Institute of Standards and Technology) XPS database [27], the Y 3d core level in Y₂(SO₄)₃ was fixed to the range of 158.9–160 eV. Other binding energies (except the double splitting) were left to be adjusted automatically.
- The FWHM (Full Width at Half Maximum) of the Y 3d peaks was limited to 1.10 eV in order to keep the peaks uniform.

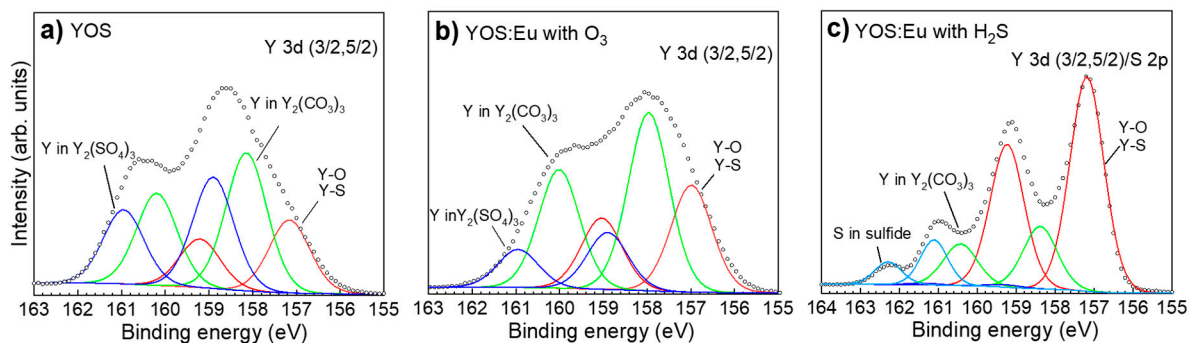


Figure 4. Measured and fitted Y 3d core level spectra in (a) undoped Y₂O_{3-x}S_x and (b) Y₂O_{3-x}S_x:Eu prepared using the Eu(thd)₃/O₃ pulse sequence. (c) Measured and fitted Y 3d/S 2p spectra in Y₂O_{3-x}S_x:Eu prepared using the Eu(thd)₃/H₂S pulse sequence. Open symbols represent measured spectra, whereas continuous lines show fitting results.

Note that, compared with other compounds, the concentration of Y₂(SO₄)₃ was very low in the sample prepared using the Eu(thd)₃/H₂S pulse sequence. Therefore, Y₂(SO₄)₃-related spectra are not visible in Figure 4c.

Table 3 summarizes the binding energies of fitted Y 3d and S 2p doublets deduced for the different samples. Based on the fitting results, the composition of the films was found to be strongly dependent on the deposition process, especially the doping configuration. The spectra were assigned to Y–O and/or Y–S bonds [25,27], Y₂(CO₃)₃ [25], Y₂(SO₄)₃ [27], and sulfur in sulfide form [27]. While Y–O/Y–S and Y₂(CO₃)₃ were present in all films, S 2p doublets ranging between 160 and 164 eV were only found in the YOS:Eu sample grown using the Eu(thd)₃/H₂S sequence. A comparison of the relative amount of the identified yttrium compounds showed that the undoped YOS and the YOS:Eu prepared using the Eu(thd)₃/O₃ pulse sequence had the highest concentration of Y₂(CO₃)₃, with relative amounts of 42.86% and 52.08%, respectively, while the YOS:Eu film prepared using the Eu(thd)₃/H₂S pulse had a relative Y₂(CO₃)₃ amount of 16.23%.

Table 3. Binding energy for Y 3d and S 2p doublets deduced for the compounds present in the Y₂O_{3-x}S_x and Y₂O_{3-x}S_x:Eu films prepared by processes P0, P2, and P3.

Process	Y–O/Y–S		Y ₂ (CO ₃) ₃		Y ₂ (SO ₄) ₃		Sulfide	
	Y 3d 5/2 (eV)	Y 3d 3/2 (eV)	Y 3d 5/2 (eV)	Y 3d 3/2 (eV)	Y 3d 5/2 (eV)	Y 3d 3/2 (eV)	S 2p 3/2 (eV)	S 2p 1/2 (eV)
P0	157.16	159.21	158.14	160.19	158.90	160.95	-	-
P2	156.98	159.03	157.96	160.01	158.90	160.95	-	-
P3	157.18	159.23	158.38	160.43	159.30	161.35	161.11	162.29

3.3. Photoluminescence

Figure 5a shows the photoluminescence spectra for YOS:Eu samples prepared using either the $\text{Eu}(\text{thd})_3/\text{O}_3$ or the $\text{Eu}(\text{thd})_3/\text{H}_2\text{S}$ pulse sequence. The measurements were carried out at room temperature and both samples were excited with wavelengths of 266 and 330 nm. For an excitation wavelength of 330 nm, the $\text{Y}_2\text{O}_{3-x}\text{S}_x$:Eu sample prepared using O_3 showed no significant emission. However, for an excitation wavelength of 266 nm, luminescence spectra between 550 and 720 nm were obtained. The highest emission intensity was obtained at about 618 nm. Unlike the sample prepared using O_3 , for an excitation wavelength of 266 nm, the $\text{Y}_2\text{O}_{3-x}\text{S}_x$:Eu sample prepared using H_2S exhibited a dominant broad emission band below 500 nm. This band shape was dependent on the excitation wavelength. Thus, when the excitation wavelength was increased from 266 to 330 nm, the shoulder located at about 440 nm became more dominant than the one at about 420 nm. Figure 5b shows the 1931 CIE color coordinates deduced from the PL measurements using OriginLab Chromaticity Diagram script (Origin Pro 2019, Northampton, MA, USA). Thus, processes P2 and P3 led to the (x, y) values of (0.490, 0.303) and (0.165, 0.060), respectively.

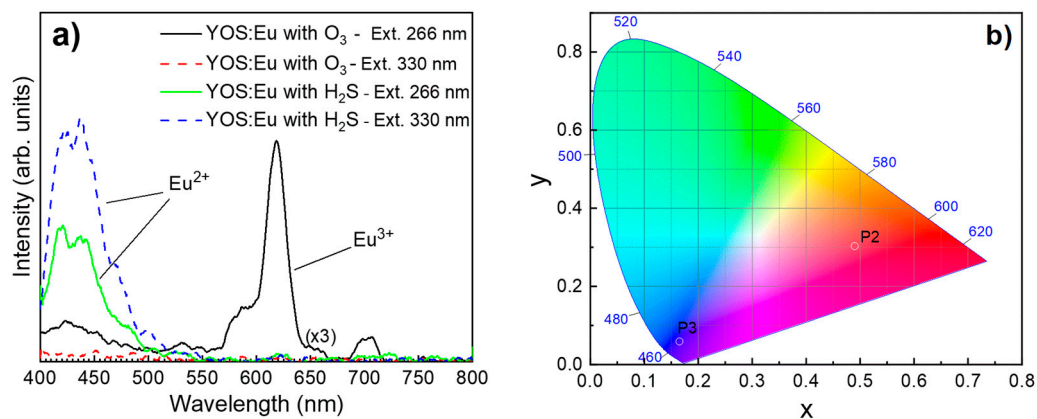


Figure 5. (a) Photoluminescence spectra measured from $\text{Y}_2\text{O}_{3-x}\text{S}_x$:Eu samples prepared using either process P2 or P3. The measurements were carried out at room temperature. Excitation wavelengths of 266 and 330 nm were used. (b) CIE 1931 chromaticity diagram for $\text{Y}_2\text{O}_{3-x}\text{S}_x$:Eu samples deduced from photoluminescence measurements in (a).

4. Discussion

$\text{Y}_2\text{O}_{3-x}\text{S}_x$:Eu thin films were successfully grown at 300 °C using ALD. The different characterization tools showed that the structural and emission properties of the obtained films depended strongly on the pulse sequences, especially the doping configuration. After each $\text{Eu}(\text{thd})_3/\text{O}_3$ pulse sequence, the introduction of a subsequent H_2O pulse improved the homogeneity of the films, as H_2O is known to contribute to the increase of OH surface group concentration [28], most likely promoting the surface adsorption of yttrium species.

As expected, the films grown using the $\text{Eu}(\text{thd})_3/\text{O}_3$ pulse sequence were found to have higher oxygen content in comparison with the ones grown using the $\text{Eu}(\text{thd})_3/\text{H}_2\text{S}$ sequence. However, the Eu concentration was lower in the films grown using O_3 , which indicates a much higher reactivity between surface Eu species and H_2S , compared to O_3 . In addition to the $\text{Y}_2\text{O}_{3-x}\text{S}_x$ phase, $\text{Y}_2(\text{CO}_3)_3$ and either $\text{Y}_2(\text{SO}_4)_3$ or sulfide compound were detected in all films, suggesting a rather complex film structure. The very high carbon concentration calculated from XPS spectra was due to $\text{Y}_2(\text{CO}_3)_3$ and surface contamination, as no special precautions were taken to protect the film surface after the processes. Carbon contamination was most likely higher on the surface of YOS:Eu samples grown using the $\text{Eu}(\text{thd})_3/\text{H}_2\text{S}$ pulse sequence, considering their crystalline nature and therefore their larger surface area. Moreover, the concentration of carbonates measured by XPS also correlated with the crystalline structure of the films: unlike the highly polycrystalline structure of films grown using H_2S , the undoped

$Y_2O_{3-x}S$ films as well as $Y_2O_{3-x}S:Eu$ grown using O_3 contained a large amount of yttrium carbonates. This is consistent with reports in which the crystallinity of Y_2O_3 thin films was improved by annealing the samples and therefore reducing the amount of carbonates in the films [29,30].

In addition to the Y–O/Y–S expected bonds, $Y_2(SO_4)_3$ was identified in films grown using the $Eu(thd)_3/O_3$ sequence, whereas in the ones grown using the $Eu(thd)_3/H_2S$ pulse sequence, S 2p doublets were found in the (160–164) eV energy range. The latter hints to the formation of a pure sulfide compound. It is therefore speculated that EuS species were most likely present in the films grown using the $Eu(thd)_3/H_2S$ pulse sequence, considering that Eu atoms were deliberately exposed to the reducing H_2S gas (i.e., $H_2S/Eu(thd)_3/H_2S$ pulse sequence) in order to generate a divalent oxidation state of Eu.

The samples were excited with energies (wavelengths of 266 and 330 nm) that were lower than the band gap of Y_2O_2S ($E_g \approx 5$ eV). Therefore, the energy of the incident photons was too low to excite the YOS lattice. As a result, luminescent centers were excited directly. In the case of the $Y_2O_{3-x}S_x:Eu$ sample prepared using O_3 , for an excitation wavelength of 266 nm, the typical $Eu^{3+} {}^5D_0 \rightarrow {}^7F_J$ ($J = 0, 1, 2, 3,$ and 4) transitions were activated, resulting in red/pink emission spectra between 550 and 720 nm, the sharp and strong emission intensity of the ${}^5D_0 \rightarrow {}^7F_2$ electronic transition being located at about 618 nm. For excitation wavelengths of both 266 and 330 nm, the $Y_2O_{3-x}S_x:Eu$ sample prepared using H_2S showed a single broad blue/violet emission below 500 nm that most likely originated from the $4f^65d \rightarrow 4f^7$ electronic transitions of Eu^{2+} ions. The shape and intensity dependence of the Eu^{2+} -related emission on the excitation wavelength, which has also been reported by other authors [31,32], suggests that the Eu^{2+} activator may be taking different kinds of ion sites in the host lattice [32].

5. Conclusions

In this work, $Y_2O_{3-x}S_x:Eu$ thin films were grown by atomic layer deposition. The crystallinity, composition, and emission properties of the obtained phosphors were correlated with the preparation conditions. XPS measurements showed the presence of $Y_2(CO_3)_3$ and either $Y_2(SO_4)_3$ or sulfide compounds, in addition to $Y_2O_{3-x}S_x$. The use of $Eu(thd)_3$ in combination with H_2S led to films with a crystalline structure. It was shown that the oxidation state of Eu in the host matrix could be successfully controlled through the doping configuration, and a violet/blue $Y_2O_{3-x}S_x:Eu$ phosphor was demonstrated. Red/pink emission was obtained when the Eu dopant was deliberately exposed to oxidizing O_3 , whereas a violet/blue emission was obtained when Eu was exposed to the reducing H_2S gas.

Author Contributions: Conceptualization, S.M.; Formal analysis, J.R., J.D., and S.M.; Investigation, J.R., J.D., P.J.S., M.B., and Z.Z.; Resources, E.F., R.M., and M.S.; Writing—original draft preparation, J.R. and S.M.; Writing—review and editing J.R., P.J.S., and S.M.; Supervision, S.M. All authors have read and agreed to the published version of the manuscript.

Funding: The work in this paper was funded by the European Union’s Horizon 2020 research and innovation programme under the Marie Skłodowska-Curie grant agreement No 764951 and project UID/CTM/50025/2019; by the FCT-MCTES and FEDER funds through the COMPETE 2020 Programme; and by the National Funds through FCT—Portuguese Foundation for Science and Technology under project number POCI-01-0145-FEDER-007688, Reference UID/CTM/50025, as well as PTDC/NAN-MAT/30812/2017 (Project NeurOxide).

Acknowledgments: The authors would like to thank Yuta Ando for the technical support and Erik Østreg and Ville Malinen for the constructive discussions.

Conflicts of Interest: The authors declare no conflicts of interest. The funders had no role in the design of the study; in the collection, analyses, or interpretation of data; in the writing of the manuscript; or in the decision to publish the results.

References

1. Wu, X.; Liu, W.; Li, J.G.; Zhu, Q.; Li, X.; Sun, X. Sulfate Exchange of the Nitrate-Type Layered Hydroxide Nanosheets of $Ln_2(OH)_5NO_3 \cdot nH_2O$ for Better Dispersed and Multi-color Luminescent Ln_2O_3 Nanophosphors ($Ln = Y_{0.98}RE_{0.02}$, RE = Pr, Sm, Eu, Tb, Dy, Ho, Er, and Tm). *Nanoscale Res. Lett.* **2016**, *11*, 1–11. [CrossRef]

2. Li, G.; Hou, Z.; Peng, C.; Wang, W.; Cheng, Z.; Li, C.; Lian, H.; Lin, J. Electrospinning derived one-dimensional LaOCl:Ln³⁺ (Ln = Eu/Sm, Tb, Tm) nanofibers, nanotubes and microbelts with multicolor-tunable emission properties. *Adv. Funct. Mater.* **2010**, *20*, 3446–3456. [[CrossRef](#)]
3. Bünzli, J.C.G. Rising Stars in Science and Technology: Luminescent Lanthanide Materials. *Eur. J. Inorg. Chem.* **2017**, *2017*, 5058–5063. [[CrossRef](#)]
4. Li, G.; Lin, J. Recent progress in low-voltage cathodoluminescent materials: Synthesis, improvement and emission properties. *Chem. Soc. Rev.* **2014**, *43*, 7099–7131. [[CrossRef](#)] [[PubMed](#)]
5. Yuan, G.; Li, M.; Yu, M.; Tian, C.; Wang, G.; Fu, H. In situ synthesis, enhanced luminescence and application in dye sensitized solar cells of Y₂O₃/Y₂O₂S:Eu³⁺ nanocomposites by reduction of Y₂O₃:Eu³⁺. *Sci. Rep.* **2016**, *6*, 37133. [[CrossRef](#)]
6. Binnemans, K. Interpretation of europium(III) spectra. *Coord. Chem. Rev.* **2015**, *295*, 1–45. [[CrossRef](#)]
7. Dorenbos, P. Energy of the first 4f⁷ → 4f⁶5d transition of Eu²⁺ in inorganic compounds. *J. Lumin.* **2003**, *104*, 239–260. [[CrossRef](#)]
8. Yu, R.; Gao, Z.; Deng, H.; Jeong, J.H. Synthesis and spectroscopic properties of Eu²⁺-activated Ba₂Zn₇F₁₈ phosphors. *J. Lumin.* **2017**, *192*, 794–800. [[CrossRef](#)]
9. Rudolph, D.; Wylezich, T.; Sontakke, A.D.; Meijerink, A.; Goldner, P.; Netzs, P.; Höpfe, H.A.; Kunkel, N.; Schleid, T. Synthesis and optical properties of the Eu²⁺-doped alkaline-earth metal hydride chlorides AE₇H₁₂Cl₂ (AE = Ca and Sr). *J. Lumin.* **2019**, *209*, 150–155. [[CrossRef](#)]
10. Shalaev, A.A.; Shendrik, R.; Myasnikova, A.S.; Bogdanov, A.; Rusakov, A.; Vasilkovskiy, A. Luminescence of BaBrI and SrBrI single crystals doped with Eu²⁺. *Opt. Mater.* **2018**, *79*, 84–89. [[CrossRef](#)]
11. Yu, C.; Cao, M.; Yan, D.; Lou, S.; Xia, C.; Xuan, T.; Xie, R.J.; Li, H. Synthesis of Eu²⁺/Eu³⁺ Co-Doped Gallium oxide nanocrystals as a full colour converter for white light emitting diodes. *J. Colloid Interface Sci.* **2018**, *530*, 52–57. [[CrossRef](#)] [[PubMed](#)]
12. Yu, H.J.; Chung, W.; Park, S.H.; Kim, J.; Kim, S.H. Luminous properties of Sr_{1-x}Zn_xSe:Eu₂ phosphors for LEDs application. *J. Cryst. Growth* **2011**, *326*, 77–80. [[CrossRef](#)]
13. Kodama, S.; Kurosawa, S.; Yamaji, A.; Pejchal, J.; Král, R.; Ohashi, Y.; Kamada, K.; Yokota, Y.; Nikl, M.; Yoshikawa, A. Growth and luminescent properties of Ce and Eu doped Cesium Hafnium Iodide single crystalline scintillators. *J. Cryst. Growth* **2018**, *492*, 1–5. [[CrossRef](#)]
14. Wang, S.; Song, Z.; Kong, Y.; Xia, Z.; Liu, Q. Crystal field splitting of 4fⁿ⁻¹5d-levels of Ce³⁺ and Eu²⁺ in nitride compounds. *J. Lumin.* **2018**, *194*, 461–466. [[CrossRef](#)]
15. Selishchev, A.V.; Pavlishchuk, V.V. Luminescence and Spectral Characteristics of Zinc Sulfide Nanoparticles Doped with Eu²⁺. *Theor. Exp. Chem.* **2016**, *51*, 366–374. [[CrossRef](#)]
16. Korir, P.C.; Dejene, F.B. The effect of deposition time on the structural, morphological and luminescence properties of Y₂O₂S:Eu³⁺ thin films prepared by pulsed laser deposition. *Appl. Phys. A Mater. Sci. Process.* **2018**, *124*, 1–9. [[CrossRef](#)]
17. Guo, C.; Luan, L.; Chen, C.; Huang, D.; Su, Q. Preparation of Y₂O₂S:Eu³⁺ phosphors by a novel decomposition method. *Mater. Lett.* **2008**, *62*, 600–602. [[CrossRef](#)]
18. Liu, X.; Pan, L.; Li, J.; Yu, K.; Sun, Z.; Sun, C.Q. Light down-converting characteristics of ZnO-Y₂O₂S:Eu³⁺ for visible light photocatalysis. *J. Colloid Interface Sci.* **2013**, *404*, 150–154. [[CrossRef](#)]
19. Wang, L.; Dong, J.; Huang, P.; Cui, C.E. Influence of sulfuretted temperature on the luminescent properties of Y₂O₂S:Eu³⁺, Mg²⁺, Ti⁴⁺ nanoarrays by EDTA complexing sol-gel template method. *J. Alloys Compd.* **2014**, *589*, 330–335. [[CrossRef](#)]
20. Behrendt, M.; Szczodrowski, K.; Mahlik, S.; Grinberg, M. High pressure effect on charge transfer transition in Y₂O₂S:Eu³⁺. *Opt. Mater.* **2014**, *36*, 1616–1621. [[CrossRef](#)]
21. Cheng, B.M.; Duan, C.K.; Tanner, P.A. Vacuum ultraviolet and visible spectra of Eu³⁺ in Y₂O₂S and Eu₂O₂S. *Opt. Mater. (Amst.)* **2009**, *31*, 902–904. [[CrossRef](#)]
22. Harazono, T.; Adachi, R.; Shimomura, Y.; Watanabe, T. Firing temperature dependence of Eu diffusion in Eu-Y₂O₂S studied by ⁸⁹Y MAS NMR. *Phys. Chem. Chem. Phys.* **2001**, *3*, 2943–2948. [[CrossRef](#)]
23. Hardy, A.E. The Performance Characteristics of Yttrium Oxysulfide—A New Red Phosphor for Color Television. *IEEE Trans. Electron. Dev.* **1968**, *15*, 868–872. [[CrossRef](#)]

24. Wang, X.; Li, J.G.; Zhu, Q.; Li, X.; Sun, X.; Sakka, Y. Facile and green synthesis of $(\text{La}_{0.95}\text{Eu}_{0.05})_2\text{O}_2\text{S}$ red phosphors with sulfate-ion pillared layered hydroxides as a new type of precursor: Controlled hydrothermal processing, phase evolution and photoluminescence. *Sci. Technol. Adv. Mater.* **2014**, *15*, 014204. [[CrossRef](#)] [[PubMed](#)]
25. Crist, B.V. Commercially Pure Binary Oxides (Ag-B, Zn-Zr Only) and a Few Common Carbonates and Hydroxides. In *Handbooks of Monochromatic XPS Spectra*; XPS International, LLC: Mountain View, CA, USA, 2005; pp. 795–810.
26. XPS Simplified: XPS Data Interpretation. Available online: <https://xpssimplified.com/whatisxps.php> (accessed on 17 June 2019).
27. Alexander, V.N.; Anna, K.-V.; Stephen, W.G.; Cedric, J.P. NIST X-ray Photoelectron Spectroscopy Database. Available online: <https://srdata.nist.gov/xps/> (accessed on 17 June 2019).
28. Puurunen, R.L. Surface chemistry of atomic layer deposition: A case study for the trimethylaluminum/water process. *J. Appl. Phys.* **2005**, *97*, 121301. [[CrossRef](#)]
29. Malek Khachatourian, A.; Golestani-Fard, F.; Sarpoolaky, H.; Vogt, C.; Zhao, Y.; Toprak, M.S. Green Synthesis of $\text{Y}_2\text{O}_3\text{:Eu}^{3+}$ Nanocrystals for Bioimaging. *MRS Proc.* **2015**, *1720*, 59–64. [[CrossRef](#)]
30. Wnag, X.; Hu, Y.; Meng, X.; Li, Y.; Zhu, M.; Jin, H. Synthesis of Y_2O_3 phosphor by a hydrolysis and oxidation method. *J. Rare Earths* **2015**, *33*, 706–711. [[CrossRef](#)]
31. Avci, N.; Korthout, K.; Newton, M.A.; Smet, P.F.; Poelman, D. Valence states of europium in $\text{CaAl}_2\text{O}_4\text{:Eu}$ phosphors. *Opt. Mater. Express* **2012**, *2*, 321. [[CrossRef](#)]
32. He, H.; Song, X.; Fu, R.; Pan, Z.; Zhao, X.; Deng, Z.; Cao, Y. Crystal structure and luminescence of $\text{Li}_2\text{Ca}_{0.7}\text{Sr}_{0.3}\text{SiO}_4\text{:Eu}^{2+}$ and its application in multi-phosphor converted white LEDs. *J. Alloys Compd.* **2010**, *493*, 401–405. [[CrossRef](#)]



© 2019 by the authors. Licensee MDPI, Basel, Switzerland. This article is an open access article distributed under the terms and conditions of the Creative Commons Attribution (CC BY) license (<http://creativecommons.org/licenses/by/4.0/>).